Journal on Electronic and Automation Engineering

Vol: 3(1), March 2024

REST Publisher; ISSN: 2583-6951 (Online)

Website: https://restpublisher.com/journals/jeae/

DOI: https://doi.org/10.46632/jeae/3/1/10

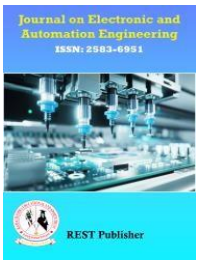

Noise Shaping SAR ADC Using 2nd order Passive Integrator

*** N. Viswanathan, C. Arunprasath, G. Nagalalli, D. Karthickraj**

Mahendra Engineering College, Namakkal, Tamil Nadu, India.

*Corresponding author: **coe@mahendra.info**

Abstract: *A wide description of Noise-Shaping (NS) Successive Approximation Register (SAR) Analog-to-Digital converters (ADC) is presented, which includes basic concepts, functional rules, and essential NS SAR layouts. The NS SAR additionally does zeros minimization on the Noise Transfer Function (NTF). The projected technique improves the Signal-to-Noise Ratio (SNR) of the suggested NS SAR ADC model by lowering the kT/C noise and the rate of conversion. The whole design is simple and sturdy, requiring just modest changes to the typical SAR ADC. This brief suggests a comparator-based 2nd order proposed model that utilizes two distinct passive integrators. The layout of fluid comparators is discussed, emphasizing its importance in the SAR ADC scheme. The suggested ADC has a maximum Schreier figure of qualities (FoMs) of 171.9 dB, a 78.69-dB Signal-to-Noise-and-Distortion Ratio (SNDR), and an Over-Sampling Ratio (OSR) of 8.*

Keywords: *NS, SAR, NTF, ADC, Integrator*

1. INTRODUCTION

The increasing requirement for multiple uses in low-power devices, as glowing as the necessity to recover series life, have strained the abilities of any ADC to their limits in the twenty-first century [1-3]. Modern technologies use tiny voltages (<1.1 V), making it challenging to meet both industries and their needs. The problem is to create structures that can withstand the impact of all of these kinds of mistake. Multiple kinds of ADCs have been developed carried out for pushing their capabilities to the restrict and satisfy the needs for every application; notable is the pursuit for small influence requirements and a sufficient number of bits, which affect the SNDR and OSR, between additional features. It is value observing that a quantity of these parameters is connected; Figure 1 depicts the primary ADC designs with regard to of frequency and sharpness [4-8]. The SAR ADC constitutes one of the most commonly used ADC designs. It has moderate quality and is straightforward to build [9–12]. Yet, for excellent quality uses, power efficiency suffers due to rigorous demands on comparison noise and an exponentially larger capacitor DAC array. The proposed model is a recently created hybrid ADC design that brings together the aids of SAR and Sigma-Delta ADCs [13-16]. The proposed model considerably decreases within the band comparative and quantization noise while maintaining its energy consumption [17, 18]. The Comparator noise is an important element in SNR. Because of their simple construction and less power use, dynamic comparators have become more commonly utilized in SAR ADCs than statically comparators. Yet, due to their low gain, dynamic comparators have higher input referred noise than static comparators. While the comparator clatter is formed in proposed model, it is still too big for excellent quality applications. Multiple approaches have been implemented developed to reduce it. The spurious free dynamic range (SFDR) and SNR improvement method is suggested [19-21], which compares the Least Significant Bit (LSB) utilizing redundancy DAC with the mean comparator noise. The Majority Voting (MV) technique has been suggested [22,23], while a tri-level elective method is used [24] to effectively minimize comparator clamor and boost lower-bits judgment correctness. Yet, these methods occur at the penalty of a reduced frequency of sampling. For particular uses, minimizing electricity use is critical, and SAR is the most efficient coefficient because of the decreased equipment used in its building, as illustrated in Figure 2, which plots influence ingesting in contradiction of sampling the frequency rate fs, in proposed model, and Sigma Delta (SD) executions, compared with Continuous-Time (CT) and Switched-Capacitor (SC) [25].

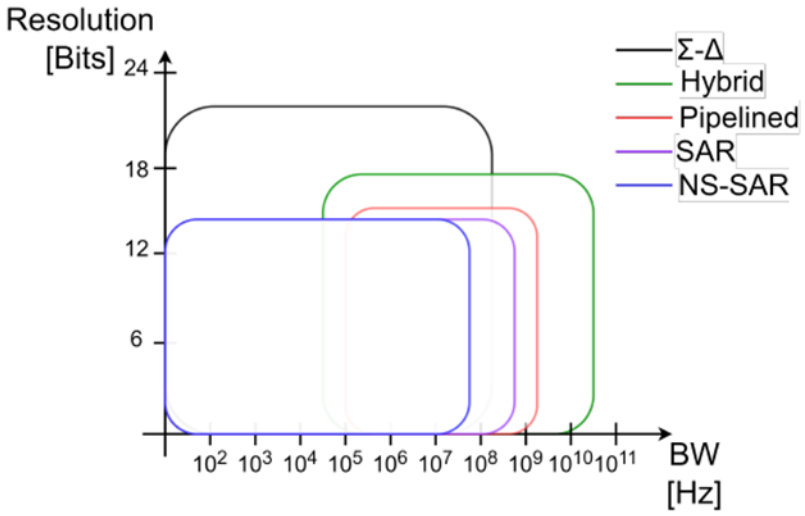

FIGURE 1. Comparison of ADC types based on BW and sharpness

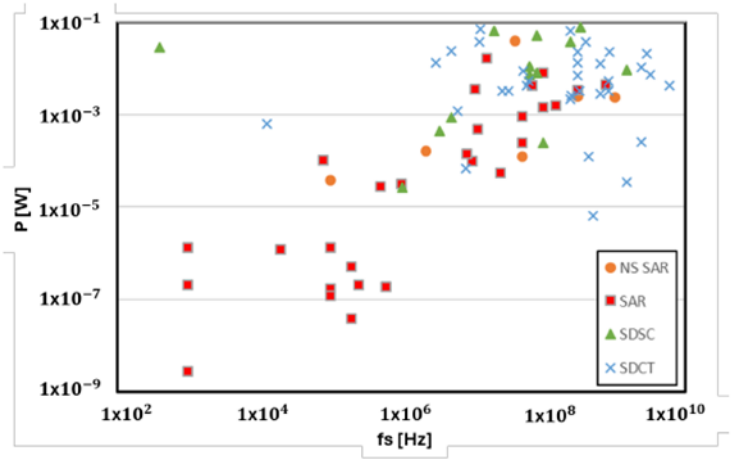

FIGURE 2. An examination of electrical usage between standard A/D C designs and NS-SARs.

The NS impact is achieved by screening and sending back recently converted residue. Similarly to the ADC, the condition of the looping filter has a direct impact on the NS efficiency of the proposed model. The initial suggested method was described in [26]. A sharp NTF is obtained by using an Operational Transconductance Amplifier (OTA). Nevertheless, the usage of high-gain, fast-settling OTA will adversely impact the use of electricity. To reduce electricity, the researchers in [27-29] used Dynamic Amplifiers (D-Amps) rather than OTAs. Nonetheless, the D-Amp's gain is sensitive to operation, current, voltage and humidity fluctuations. Loop filters may additionally be built into passive switched-capacitor circuits to improve reliability and NS robustness [30-33]. Because the NTFs are all determined by constituent ratios, they are immune to PVT fluctuations. Entirely inactive filters are easy, low-power, and reliable, but their NS characteristics are limited by noisy Passive Integrator (PI) [30]. [32] achieves a high second-order NTF using a three-input-path latch-based comparator. However, the additional two input lines will reduce distortion efficiency, and the huge integration capacitance will boost the ADC zone. In this short, we present a comparator-based 2nd order passive proposed model. Two passive integrators are used to incorporate what remains on the 9-bit DAC repeatedly. The primary and next integral outcomes are sent into the comparator, which performs active accumulation and translation. The comparator contains a second passive integrator that is incorporated using Output Offset Storage (OOS) technology [34]. The dimension of the 2nd order PI varies independently of the initial one, and it can be lowered to increase area effectiveness. To mitigate the effects of capacitor inconsistency, the Data Weighted Averaging (DWA) approach [35] is used,

2. THE SUGGESTED 2ND ORDER FULLY PASSIVE PROPOSED MODEL

Some previous studies used OTA to create active filter elements with an acceptable NS effect [17]. Yet, OTA uses a lot of energy and is not suitable for scalability. In the past few years, approaches for implementing totally passive filters using switching and capacitors have been suggested [36, 37]. These passive SC filters are effortless, low-power, reliable, and adaptable. Figures 3(a) and (b) demonstrate past work on 2nd order fully-passive proposed model. Pursuant to the information flow pattern depicted in Figure 1, Vint1 and Vint2 can be generated using equations (1) and (2):

$$V_{int}(Z) = (1-a)\frac{a}{1-(1-a)Z^{-1}}V_{res}(z) \quad (1)$$

$$V_{int}(z) = \frac{a}{1-(1-a)z^{-1}}V_{int1}(z) = (1-a)\frac{a^2}{[1-(1-a)z^{-1}]^2}V_{res}(z) \quad (2)$$

where the enduring voltage is $V_{res}(z) = V_{in}(z) - D_{OUT}(z)$.

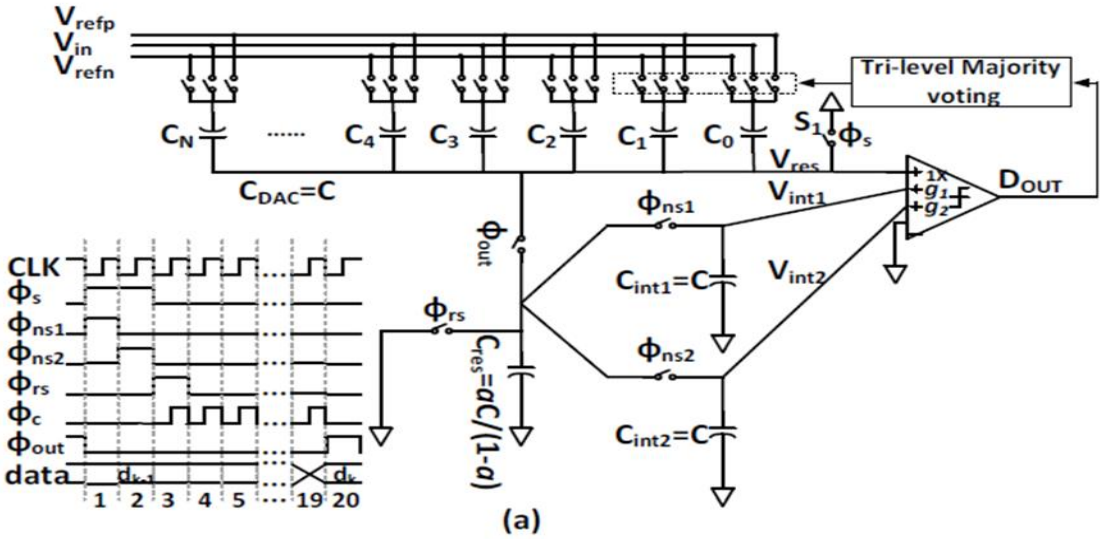

FIGURE 3. (a) 2nd order passive proposed model Design

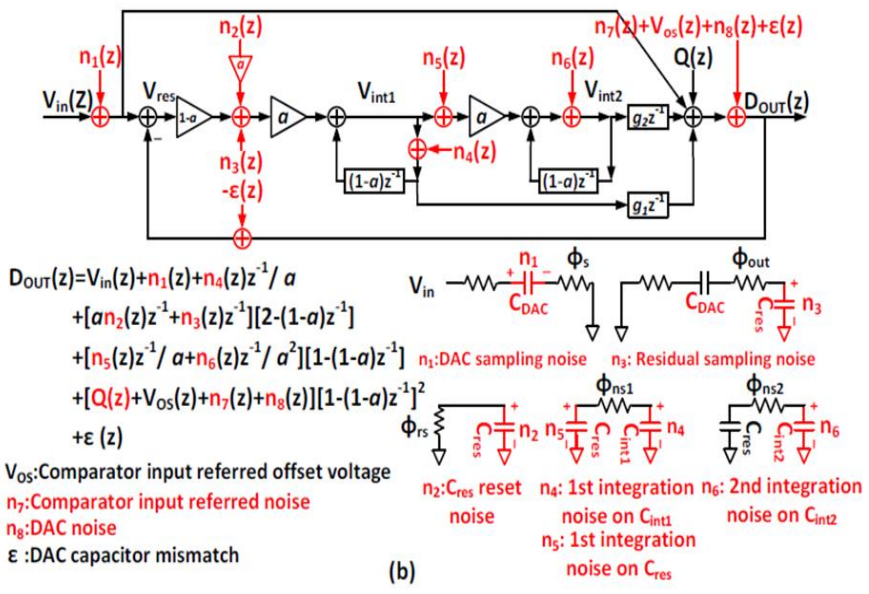

FIGURE 3 (b). Signaling flow chart

The linking among input and output can be mentioned as in Equation (3):

$$D_{OUT}(z) = V_{in}(z) + g_1 Z^{-1} V_{int1}(z) + g_2 Z^{-1} V_{int2}(z) + Q(z) \quad (3)$$

Q(z) represents quantum noise. By substituting (1) and (2) into (3), the preceding NS SAR ADC's z-domain TF with only quantization noise may be derived in equation (4) as follows:

$$D_{OUT}(z) = \frac{V_{in}(z)+\left[1-(1-a)z^{-1}\right]^2}{1+(1-a)(g_2a^2+g_1a-2)z^{-1}+(1-a)^2(1-g_1a)z^{-2}} Q(z) \quad (4)$$

Figure 1 shows common values for a, g1, g2, and OSR as 1/4, 4, 16, and 16, accordingly. Since it is proportional to capacitors, the parameter an is resistant to fluctuations in Process Voltage and Temperature (PVT). The values of g1 and g2 define the comparative assets of the comparator's various input pairs and are immune to PVT changes and errors. Nevertheless, fluctuations in g1 and g2 with PVT have no effect on the structure's equilibrium, which is being thoroughly investigated.

The values of a, g1, and g2 might be influenced by PVT changes and incompatibilities during production. Yet, a, g1, and g2 are treated as constants in the next evaluation as differences in PVT and incompatibilities are disregarded. As a outcome, the z-domain TF, which includes only quantized noise, can be reduced in equation (5) as follows:

$$D_{OUT}(z) = V_{in}(z) + \left[1 - \frac{3}{4}z^{-1}\right]^2 Q(z) \quad (5)$$

Excluding extraneous noises, the enhanced ideal Effective Number of Bits (ENOBs), also known as ENOBimp, can be represented as (6).

$$ENOB_{imp} = \frac{-10\log\left(\frac{1}{256OSR}+\frac{\pi^2}{32}\frac{1}{OSR^3}+\frac{3.6\pi^4}{32}\frac{1}{OSR^5}\right)}{6.02} \quad (6)$$

Utilizing comparable methods, the inside the band noise powers of various sources of sound can be determined. Within the band noise strength $n_{1\_ib}^2 - n_{6\_ib}^2$ are approximately $n_1^2\ /OSR$,$[0.1 + \pi^2/(32OSR^2)n_2^2/OSR, [1.56 + \pi^2\ /(2OSR^2)]\bar{n}_3^2$ / OSR̄, $16n_4^2$/ OSR, $[1+\ 4\pi^2/OSR^2]\ n_5^2/OSR, [16 + 64\pi^2/OSR^2]n_6^2/OSR$. It is evident that the building's NS capability varies depending on the noise. If the noise remains unaltered by NS, the influence of noise increases to 1/OSR times the initial value following oversampling.

Yet, NS only reduces low-frequency C_{res} reset noise influence by around a issue of ten, while increasing the in-band noise levels of $n_3 - n_6$. To successfully reduce kT/C noise, capacitors must be sufficiently large to support excellent quality systems. To overcome this issue, a 2nd order proposed model using dynamic gain is presented

3. THE ENHANCED 2ND ORDER PROPOSED MODEL BASED ACTIVE GAIN (AG)

To reduce the degradation of the final signal caused by noise n1, an enhanced 2nd order proposed model using AG is presented, as seen in Figure 4. The kT/C noise reduction principle introduced in [38,39] is used. $\varphi_s$is separated into φ_{sDAC} and φ_{snc}, which control switching S1 and S2, accordingly.

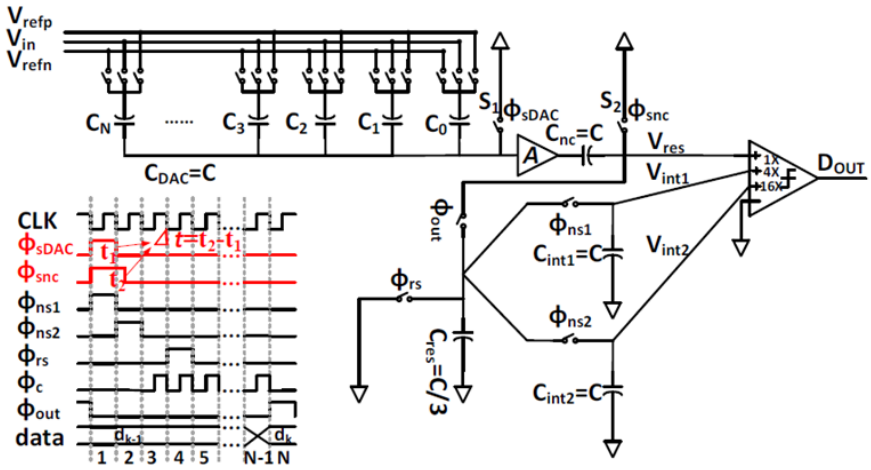

FIGURE 4. Enhanced 2nd order proposed system

The kT/C invalidation of noise method is shown in Figure 5. The sample process is separated into two parts: C_{DAC} evaluation phase and C_{nc} evaluation phase. The C_{DAC} sample phase lasts from t0 to t1, and is regulated by φ_{sDAC}. At time t1, sampled

input signal $V_{in}(t_1)$ and kT/C noise n1 are recorded on C_{DAC}. The offset level of the amplifier, V_{osamp} , is kept in the C_{nc}. φ_{snc}controls the C_{nc} sampling phase, which runs from t1 to t2. At t2, the input signal is $V_{in}(t_2)$, and that amplifier's input voltage is $V_{in}(t_2)$-$V_{in}(t_1)$- n_1- V_{osamp}. If the amplifier has unlimited bandwidth, it entirely resolves throughout the C_{nc} sampling phase. The voltage deposited on C_{nc} is given in equation (7):

$$V_{C_{nc}} = A[V_{in}(t_2) - V_{in}(t_1) - n_1 - V_{osamp}] \quad (7)$$

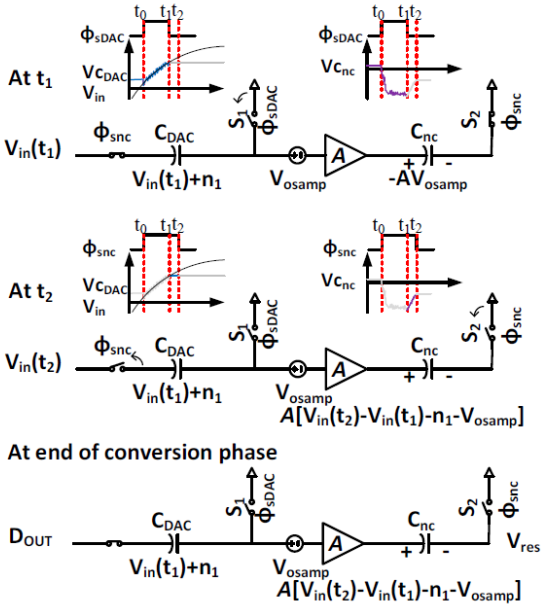

FIGURE 5. The kT/C noise cancelling principle

Abandoning capacitors C_{int1}, C_{int2}, and C_{res}, at the final stage of the conversion phase, the input-output relationship can be determined using equation (8).

$$D_{OUT} = V_{in}(t_2) + V_{res}/A \approx V_{in}(t_2) \quad (8)$$

Examining (18), it is clear that the sampled clatter n1 can be entirely cancelled if the speaker being used has unlimited bandwidth. In actuality, the amplifier's frequency is inadequate. Thus, the sampling noise amplitude deposited on C_{nc} is provided in equation (9).

$$n_1 - C_{nc} = -An_1(1 - e^{-\frac{\Delta t}{\tau}}) \quad (9)$$

where τ is the duration of the interval and the amplifier's settlement time constant [40] satisfy $\Delta t = t_2 - t_1$. The voltage stored on C_{nc} is $A\left[V_{in}(t_2) - V_{in}(t_1) - n_1\left(1 - e^{-\frac{\Delta}{\tau}}\right) - V_{osamp}\right]$.

The newly discovered input-output connection can be calculated in eq. (10) as:

$$D_{OUT} = V_{in}(t_2) + n_1 e^{-\Delta/\tau} \quad (10)$$

To reduce total capacitor in the upgraded 2nd order proposed model, rationally construct the standards of A and Δt/τ. This allows the framework to be used in excellent quality systems that do not require large-area capacitance.

To minimize noise from quantization and nevertheless preserve the NS-SAR ADC's power consumption, four capacitors such as C_S, C_{res}, C_{int1} and C_{int2} are used as 2nd order passively integrators. The multiple phases comparator, which consists of a two-path preamplifier, a dual-path dynamically latch, and a 2nd order PI, is meant to make up for the output loss of the two PI. Figures 6(a) and 6(b) illustrate the representations for the preamplifier and the active latch. g1 represents the gain ratio across the initial integrating path V_{int1} and the DAC input path V_{res}. In a comparable manner g2 is the increase in the ratio of the static latch's 2nd order integrated path V_{int2} to its signal path V_{sig}. These relative gains g1 and g2 can be achieved by merely scaling the input semiconductors, as seen in Figure 6

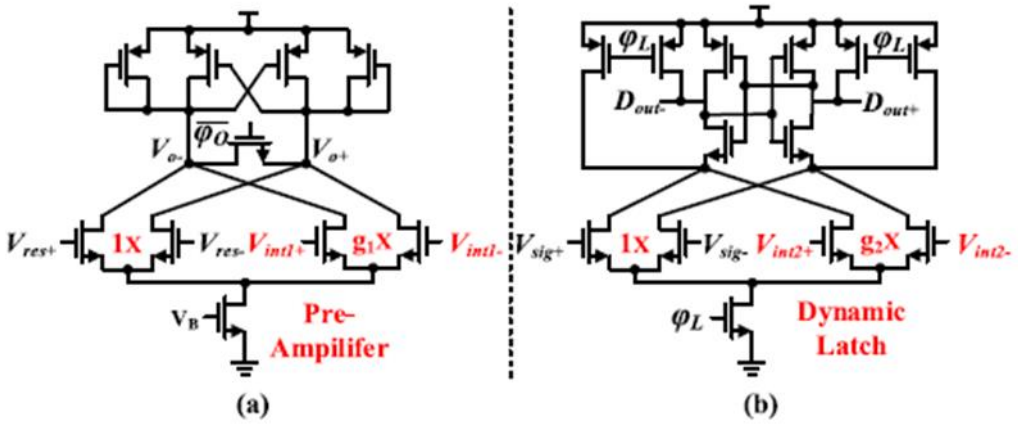

FIGURE 6. Illustration of the suggested multiple-stage comparator: (a) amplification (b) active latch.

4. RESULTS AND DISCUSSION

The nonlinearity in the DAC is caused by a capacitor incongruity, particularly manifests itself at the yield when no changes are made. DWA [35] is a robust and hardware-efficient solution for eliminating alignment errors. The thermometer processor selects unit elements sequentially from the aforementioned 4-bit MSBs, beginning with the subsequent available unoccupied component. The capacitor differential between the four-bit MSBs is optimized for the highest possible frequency. The DAC input codes have the same periodic pattern as the input signal. Mismatched capacitors cause within-band signal-dependent disturbances in the ADC input spectra [35]. To address the harmonic distortion issue, a little accidental dither is used to randomize the DAC input coding and distribute the strength of dominating vocal tones across every frequency. Yet, due to the dither's added noise the contribution, the SNDR is drastically impaired, as is the constancy of the NS track [35]. In this layout, an electronic dither is used to address this issue. Before first-bit quantization. This process the dithering capacitor CT will be linked to the voltage of reference Vrefp or Vrefn based on the binary pseudorandom number (PRN) generated by integrated-chip quadratic response shifting clock. The uncertain dither can be readily addressed after every conversion through including the PRN to the final translation codes. Though the electronic dither solitary boosts SNDR by 0.5 dB for a capacitor mismatch of 0.5%, the suggested DWA may effectively reduce the capacitor misalignment without decreasing SNDR, as demonstrated in Figure 7

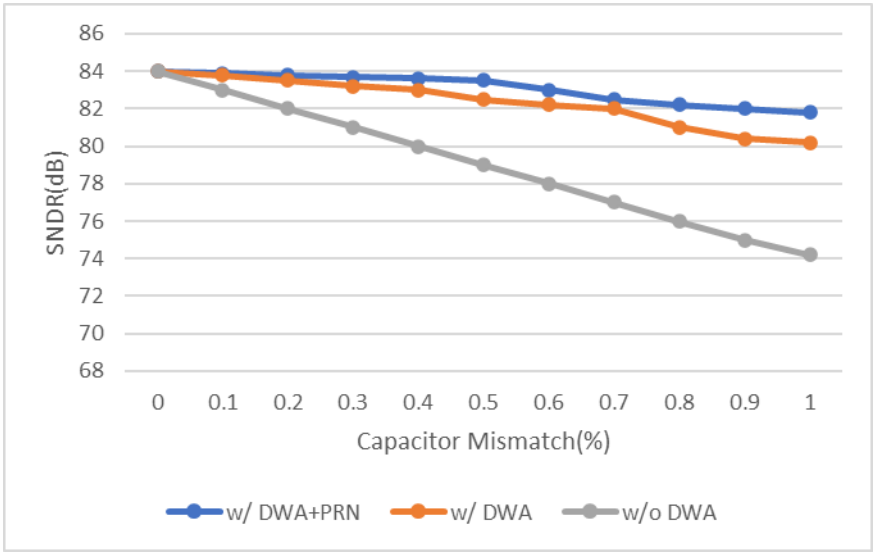

FIGURE 7. Simulated SNDR versus capacitor mismatch

5. GAIN VARIATION

Given the differences in the working setting, including supply voltage and operational humidity, the output gain of the

preamplifier AV determination fluctuates significantly throughout every SAR change. To study the impact of AV on NS competence, Figure 8(a) depicts a modelled SNDR as an expression of gain deviations, varying from 0% to 50%. Using the Hspice Tool, the greatest AV fluctuation is 3.6% across an ambient temperature range of -25°C to 125°C and an overall supply variation of ±10%. As a result, the corresponding variance in AV has little effect on the NS capabilities. Figure 8(b) depicts the effect of g1 and g2 modifications on SNDR, given that pole positions are determined by g1 and g2, respectively. If the greatest possible fluctuations of g1 and g2 are kept to 20%, which meets the level of inequality, they are far from the problematic border. According to the Monte Carlo model used in Hspice Tool, the greatest variances of g1 and g2 are 10.5% and 15.7%, etc.

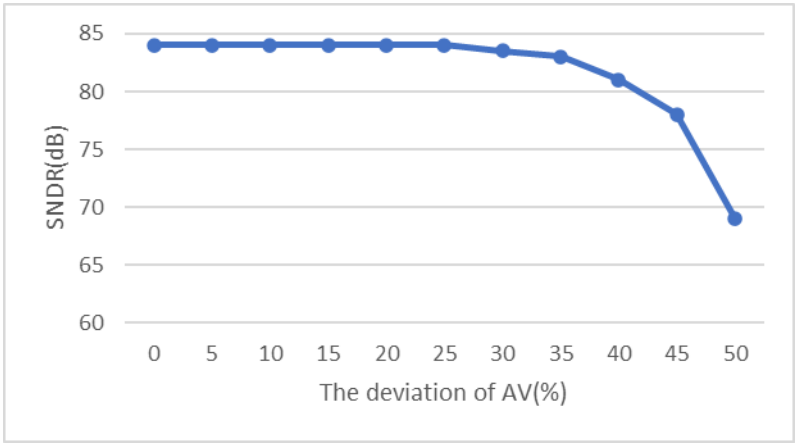

FIGURE 8(a). Modelled SNDR

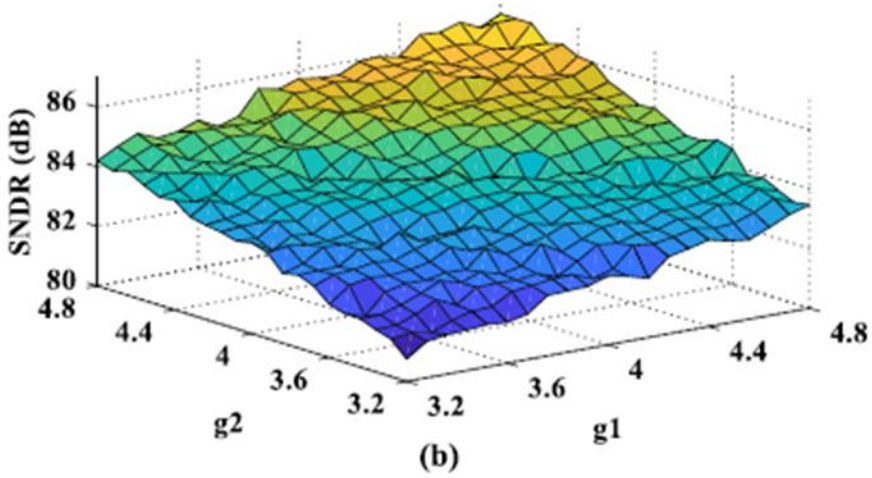

FIGURE 8(b). Simulated SNDR versus g1 and g2 variations

Figure 9 plots the generated SNDR vs input frequency as well as amplitude. The plot displays a DR of 79.1 dB, and the simulation's SNDR will be somewhat decreased when the frequency that was input approaches the BW of 125 kHz. To evaluate the vilest possible dynamical qualities of the proposed prototype at various locations and humidity, transistor-level pre- and post-layout computations deprived of and with intermittent disturbance were done

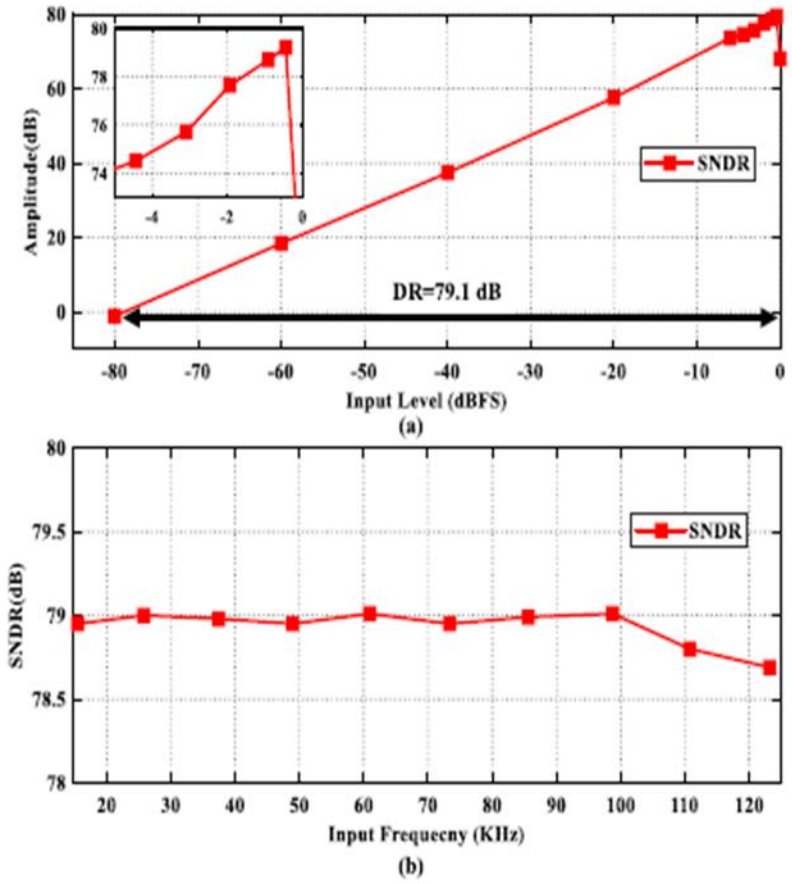

FIGURE 9. Replicated SNDR versus (a) input amplitude and (b) input frequency

6. CONCLUSION

This short-term suggests a comparator-based 2nd proposed model with two separate PI. The synthesizer can be utilized for both SAR transformation and residual intensification. The EC of the 2nd order PI can be lowered to increase area efficiency. The component ratio determines the NTF zeros and poles, resulting in resistance to PVT changes and a strong NS capacity. The suggested DWA method effectively suppresses capacitor mismatches. The proposed approach is fully scalable with increased sparsity and can be tailored to unexpected sparseness. Whereas lesser capacitance reduces dynamic energy use, the addition of an open-loop amplifier increases static electrical ingesting. This requires a trade-off among effectiveness and energy usage. This requires a compromise among effectiveness and energy usage. However, this method remains a viable option for fast speeds and high-resolution purposes. In general, the suggested architecture is simple and resilient, making it suitable for Internet of Things (IoT) scenarios.

REFERENCES

[1]. Choi, C.; Lee, J.-W. An 11.8-fJ/Conversion-Step Noise Shaping SAR ADC with Embedded Passive Gain for Energy-Efficient IoT Sensors. Sensors 2022, 22, 869. [CrossRef] [PubMed]
[2]. Chen, D.; Cui, X.; Zhang, Q.; Li, D.; Cheng, W.; Fei, C.; Yang, Y. A Survey on Analog-to-Digital Converter Integrated Circuits for Miniaturized High Resolution Ultrasonic Imaging System. Micromachines 2022, 13, 114. [CrossRef] [PubMed]
[3]. Leene, L.B.; Letchumanan, S.; Constandinou, T.G. A 68_W 31kS/s Fully-Capacitive Noise-Shaping SAR ADC with 102 dB SNDR. In Proceedings of the IEEE International Symposium on Circuits and Systems (ISCAS), Sapporo, Japan, 26–29 May 2019; pp. 1–5.
[4]. Lu, R.; Flynn, M.P. A 300MHz-BW 38mW 37dB/40dB SNDR/DR Frequency-Interleaving Continuous-Time Bandpass Delta-Sigma ADC in 28 nm CMOS. In Proceedings of the Symposium on VLSI Circuits, Kyoto, Japan, 13–19 June 2021; pp. 1–2.
[5]. Bolatkale, M.; Breems, L.J.; Rutten, R.; Makinwa, K.A.A. A 4GHz CT DS ADC with 70dB DR and □74dBFS THD in 125MHz BW. In Proceedings of the International Solid-State Circuits Conference, San Francisco, CA, USA, 20–24 February 2011; pp. 470–472.
[6]. Ginsburg, B.P.; Chandrakasan, A.P. Highly Interleaved 5b 250MS/s ADC with Redundant Channels in 65nm CMOS. In

Proceedings of the International Solid-State Circuits Conference—Digest of Technical Papers, San Francisco, CA, USA, 3–7 February 2008; pp. 240–610.
[7]. Kull, L.; Luu, D.; Menolfi, C.; Morf, T.; Francese, P.A.; Braendli, M.; Kossel, M.; Cavrero, A.; Ozkaya, I.; Toifl, T. A 10-Bit 20–40 GS/S ADC with 37 dB SNDR at 40 GHz Input Using First Order Sampling Bandwidth Calibration. In Proceedings of the Symposium on VLSI Circuits, Honolulu, HI, USA, 18–22 June 2018; pp. 275–276.
[8]. Zheng, Z.; Wei, L.; Lagos, J.; Martens, E.; Zhu, Y.; Chan, C.-H.; Craninckx, J.; Martins, R.P. 16.3 A Single-Channel 5.5 mW 3.3GS/s 6b Fully Dynamic Pipelined ADC with Post-Amplification Residue Generation. In Proceedings of the IEEE International Solid-State Circuits Conference (ISSCC), San Francisco, CA, USA, 16–20 February 2020; pp. 254–256.
[9]. Elzakker, M.v.; Tuijl, E.v.; Geraedts, P.; Schinkel, D.; Klumperink, E.A.M.; Nauta, B. A 10-bit Charge-Redistribution ADC Consuming 1.9 _Wat 1 MS/s. IEEE J. Solid-State Circuits 2010, 45, 1007–1015. [CrossRef]
[10]. Liu, C.C.; Chang, S.J.; Huang, G.Y.; Lin, Y.Z.; Huang, C.M. A 1V 11fJ/conversion-step 10bit 10MS/s asynchronous SAR ADC in 0.18_m CMOS. In Proceedings of the 2010 Symposium on VLSI Circuits, Honolulu, HI, USA, 16–18 June 2010; pp. 241–242.
[11]. Shen, Y.; Tang, X.; Shen, L.; Zhao,W.; Xin, X.; Liu, S.; Zhu, Z.; Sathe, V.S.; Sun, N. A 10-bit 120-MS/s SAR ADCWith Reference Ripple Cancellation Technique. IEEE J. Solid-State Circuits 2020, 55, 680–692. [CrossRef]
[12]. Xu, D.G.; Xu, K.K.; Xu, S.L.; Liu, L.; Liu, T. A System-Level Correction SAR ADC with Noise-Tolerant Technique. J. Circuits Syst. Comput. 2018, 27, 1850202. [CrossRef]
[13]. Obata, K.; Matsukawa, K.; Miki, T.; Tsukamoto, Y.; Sushihara, K. A 97.99 dB SNDR, 2 kHz BW, 37.1 _W noise-shaping SAR ADC with dynamic element matching and modulation dither effect. In Proceedings of the 2016 IEEE Symposium on VLSI Circuits (VLSI-Circuits), Honolulu, HI, USA, 15–17 June 2016; pp. 1–2.
[14]. Shu, Y.S.; Kuo, L.T.; Lo, T.Y. An Oversampling SAR ADC With DAC Mismatch Error Shaping Achieving 105 dB SFDR and 101 dBSNDR Over 1 kHz BW in 55 nm CMOS. IEEE J. Solid-State Circuits 2016, 51, 2928–2940. [CrossRef]
[15]. Chen, Z.; Miyahara, M.; Matsuzawa, A. A 2nd order fully-passive noise-shaping SAR ADC with embedded passive gain. In Proceedings of the 2016 IEEE Asian Solid-State Circuits Conference (A-SSCC), Toyama, Japan, 7–9 November 2016; pp. 309–312.
[16]. Li, S.; Qiao, B.; Gandara, M.; Pan, D.Z.; Sun, N. A 13-ENOB Second-Order Noise-Shaping SAR ADC Realizing Optimized NTF Zeros Using the Error-Feedback Structure. IEEE J. Solid-State Circuits 2018, 53, 3484–3496. [CrossRef]
[17]. Fredenburg, J.A.; Flynn, M.P. A 90-MS/s 11-MHz-Bandwidth 62-dB SNDR Noise-Shaping SAR ADC. IEEE J. Solid-State Circuits 2012, 47, 2898–2904. [CrossRef]
[18]. Guo, W.; Zhuang, H.; Sun, N. A 13b-ENOB 173dB-FoM 2nd-order NS SAR ADC with passive integrators. In Proceedings of the 2017 Symposium on VLSI Circuits, Kyoto, Japan, 5–8 June 2017; pp. C236–C237.
[19]. Miki, T.; Morie, T.; Matsukawa, K.; Bando, Y.; Okumoto, T.; Obata, K.; Sakiyama, S.; Dosho, S. A 4.2 mW 50 MS/s 13 bit CMOS SAR ADCWith SNR and SFDR Enhancement Techniques. IEEE J. Solid-State Circuits 2015, 50, 1372–1381. [CrossRef]
[20]. Kuo, H.L.; Lu, C.W.; Chen, P. An 18.39 fJ/Conversion-Step 1-MS/s 12-bit SAR ADC With Non-Binary Multiple-LSB-Redundantand Non-Integer-and-Split-Capacitor DAC. IEEE Access 2021, 9, 5651–5669. [CrossRef]
[21]. Jiao, Z.; Luo, H.; Zhang, J.; Wang, X.; Chen, L.; Zhang, H. An 84dB-SNDR 1-0 Quasi-MASH NS SAR with LSB Repeating and 12-bit Bridge-Crossing Segmented CDAC. In Proceedings of the 2023 IEEE Custom Integrated Circuits Conference (CICC), San Antonio, TX, USA, 23–26 April 2023; pp. 1–2.
[22]. Harpe, P.; Cantatore, E.; Roermund, A.v. A 10b/12b 40 kS/s SAR ADC with Data-Driven Noise Reduction Achieving up to 10.1b ENOB at 2.2 fJ/Conversion-Step. IEEE J. Solid-State Circuits 2013, 48, 3011–3018. [CrossRef]
[23]. Hwang, Y.H.; Song, Y.; Park, J.E.; Jeong, D.K. A Fully Passive Noise-Shaping SAR ADC Utilizing Last-Bit Majority Voting and Cyclic Dynamic Element Matching Techniques. IEEE Trans. Very Large Scale Integr. (VLSI) Syst. 2022, 30, 1381–1390. [CrossRef]
[24]. Zhuang, H.; Guo, W.; Liu, J.; Tang, H.; Zhu, Z.; Chen, L.; Sun, N. A Second-Order Noise-Shaping SAR ADC with Passive Integrator and Tri-Level Voting. IEEE J. Solid-State Circuits 2019, 54, 1636–1647. [CrossRef]
[25]. ADC Performance Survey 1997–2021. Available online: http://web.stanford.edu/~murmann/adcsurvey.html (accessed on 22 March 2022).
[26]. J. A. Fredenburg and M. P. Flynn, “A 90-MS/s 11-MHz-bandwidth 62-dB SNDR noise-shaping SAR ADC,” IEEE J. Solid-State Circuits, vol. 47, no. 12, pp. 2898–2904, Dec. 2012.
[27]. C.-C. Liu and M.-C. Huang, “A 0.46mW 5MHz-BW 79.7dB-SNDR noise-shaping SAR ADC with dynamic-amplifier-based FIR-IIR filter,” in IEEE ISSCC Dig. Tech. Papers, Feb. 2017, pp. 466–467.
[28]. M. Miyahara and A. Matsuzawa, “An 84 dB dynamic range 62.5– 625 kHz bandwidth clock-scalable noise-shaping SAR ADC with openloop integrator using dynamic amplifier,” in Proc. IEEE Custom Integr. Circuits Conf. (CICC), Apr./May 2017, pp. 1–4.
[29]. S. Li, B. Qiao, M. Gandara, D. Z. Pan, and N. Sun, “A 13-ENOB secondorder noise-shaping SAR ADC realizing optimized NTF zeros using the error-feedback structure,” IEEE J. Solid-State Circuits, vol. 53, no. 12, pp. 3484–3496, Dec. 2018.
[30]. Z. Chen, M. Miyahara, and A. Matsuzawa, “A 9.35-ENOB, 14.8 fJ/conv.- step fully-passive noise-shaping SAR ADC,” in Proc. Symp. VLSI Circuits (VLSI Circuits), Jun. 2015, pp. C64–C65.
[31]. W. Guo and N. Sun, “A 12b-ENOB 61µW noise-shaping SAR ADC with a passive integrator,” in Proc. 42nd Eur. Solid-State Circuits Conf., Sep. 2016, pp. 405–408.
[32]. H. Zhuang et al., “A second-order noise-shaping SAR ADC with passive integrator and tri-level voting,” IEEE J. Solid-State Circuits, vol. 54, no. 6, pp. 1636–1647, Jun. 2019.
[33]. Y. Zhang, S. Liu, B. Tian, Y. Zhu, C.-H. Chan, and Z. Zhu, “A 2ndorder noise-shaping SAR ADC with lossless dynamic amplifier assisted integrator,” IEEE Trans. Circuits Syst. II, Exp. Briefs, vol. 67, no. 10, pp. 1819–1823, Oct. 2020.

[34]. B. Razavi and B. A. Wooley, "Design techniques for high-speed, highresolution comparators," IEEE J. Solid-State Circuits, vol. 27, no. 12, pp. 1916–1926, Dec. 1992.
[35]. R. T. Baird and T. S. Fiez, "Linearity enhancement of multibit A/D and D/A converters using data weighted averaging," IEEE Trans. Circuits Syst. II, Analog Digit. Signal Process., vol. 42, no. 12, pp. 753–762, Dec. 1995.
[36]. Chen, Z.; Miyahara, M.; Matsuzawa, A. A 9.35-ENOB, 14.8 fJ/conv.-step fully-passive noise-shaping SAR ADC. In Proceedings of the 2015 Symposium on VLSI Circuits (VLSI Circuits), Kyoto, Japan, 17–19 June 2015; pp. C64–C65.
[37]. Guo, W.; Sun, N. A 12b-ENOB 61_W noise-shaping SAR ADC with a passive integrator. In Proceedings of the ESSCIRC Conference 2016: 42nd European Solid-State Circuits Conference, Lausanne, Switzerland, 12–15 September 2016; pp. 405–408.
[38]. Liu, J.; Tang, X.; Zhao, W.; Shen, L.; Sun, N. A 13-bit 0.005-mm2 40-MS/s SAR ADC With kT/C Noise Cancellation. IEEE J. Solid-State Circuits 2020, 55, 3260–3270. [CrossRef]
[39]. Li, H.; Youssef, M.; Shen, Y.; Cantatore, E.; Harpe, P. Analysis of the Sampling Noise Cancellation Technique in a Track-and-Hold Amplifier. In Proceedings of the 2021 28th IEEE International Conference on Electronics, Circuits, and Systems (ICECS), Dubai, United Arab Emirates, 28 November–1 December 2021; pp. 1–5.
[40]. Xu, K. Silicon electro-optic micro-modulator fabricated in standard CMOS technology as components for all silicon monolithic integrated optoelectronic systems*. J. Micromech. Microeng. 2021, 31, 054001. [CrossRef].

